

# Probing the incompressibility of nuclear matter at ultra-high density through the prompt collapse of asymmetric neutron star binaries

Albino Perego<sup>1,2</sup>, Domenico Logoteta<sup>3,4</sup>, David Radice<sup>5,6,7</sup>, Sebastiano Bernuzzi<sup>8</sup>,  
Rahul Kashyap<sup>5,6</sup>, Abhishek Das<sup>5,6</sup>, Surendra Padamata<sup>5,6</sup>, and Aviral Prakash<sup>5,6</sup>

<sup>1</sup>*Dipartimento di Fisica, Università di Trento, Via Sommarive 14, 38123 Trento, Italy*

<sup>2</sup>*INFN-TIFPA, Trento Institute for Fundamental Physics and Applications, Via Sommarive 14, I-38123 Trento, Italy*

<sup>3</sup>*Dipartimento di Fisica, Università di Pisa, Largo B. Pontecorvo, 3 I-56127 Pisa, Italy*

<sup>4</sup>*INFN, Sezione di Pisa, Largo B. Pontecorvo, 3 I-56127 Pisa, Italy*

<sup>5</sup>*Institute for Gravitation & the Cosmos, The Pennsylvania State University, University Park, PA 16802*

<sup>6</sup>*Department of Physics, The Pennsylvania State University, University Park, PA 16802*

<sup>7</sup>*Department of Astronomy & Astrophysics, The Pennsylvania State University, University Park, PA 16802 and*

<sup>8</sup>*Theoretisch-Physikalisches Institut, Friedrich-Schiller Universität Jena, 07743, Jena, Germany*

(Dated: May 18, 2022)

Using 250 neutron star merger simulations with microphysics, we explore for the first time the role of nuclear incompressibility in the prompt collapse threshold for binaries with different mass ratios. We demonstrate that observations of prompt collapse thresholds, either from binaries with two different mass ratios or with one mass ratio but combined with the knowledge of the maximum neutron star mass or compactness, will constrain the incompressibility at the maximum neutron star density,  $K_{\max}$  to within tens of percent. This, otherwise inaccessible, measure of  $K_{\max}$  can potentially reveal the presence of hyperons or quarks inside neutron stars.

PACS numbers: 04.25.D-, 97.60.Jd, 21.65.+f

*Introduction.-* The equation of state (EOS) of neutron star (NS) matter is one of the most fundamental, yet elusive, relations in physics [1, 2]. It lays at the interface between several disciplines including nuclear physics, high-energy astrophysics, heavy-ion collisions, multimessenger astronomy and gravitational wave (GW) physics. Our knowledge of NS matter properties is still partial, mostly due to the difficulties in studying strongly interacting bulk matter in the low energy limit typical of nuclear interactions [3]. Even the appropriate degrees of freedom are uncertain: while nucleons are the relevant species around the nuclear saturation density,  $n_0 = 0.16 \text{ fm}^{-3}$ , it is still unclear if hyperons [4, 5] or a phase transition to quark matter [6–8] can appear at densities  $n \gtrsim 2n_0$  in NS interiors.

NS EOS models are experimentally constrained by the masses of ordinary nuclei, as well as by the energy per baryon and its derivatives with respect to baryon density,  $n_b$ , around  $n_0$  and close to isospin symmetry, i.e. for symmetry parameter  $\delta \equiv (n_n - n_p)/n_b \approx 0$ ,  $n_{n,p}$  being the density of neutrons and protons. If  $P$  is the matter pressure, the nuclear incompressibility of cold nuclear matter at fixed composition is defined as

$$K(n_b, \delta) \equiv 9 \frac{\partial P}{\partial n_b} \Big|_{T=0, \delta=\text{const}} . \quad (1)$$

It describes the response of matter to compression and its value can be currently measured only for symmetric matter at saturation density,  $K_{\text{sat}}$ , although with some controversy [9–13]. While isoscalar giant monopole resonance experiments for closed shell nuclei provided  $K_{\text{sat}} = (240 \pm 20)\text{MeV}$ , studies based on open-shell nuclei reported quite different values in the range 250MeV–

315MeV [12] or even values around 200MeV [13]. Nevertheless,  $K_{\text{sat}}$  is unconstrained at densities and compositions relevant for NSs (far from  $n \approx n_0$  and  $\delta \approx 0$ ). In particular, the NS central density increases monotonically with the NS mass and at the stability limit, corresponding to mass and radius ( $M_{\max}^{\text{TOV}}, R_{\max}^{\text{TOV}}$ ), can reach  $n_{\max}^{\text{TOV}} \sim 4 - 7n_0$ , depending on the EOS. Moreover, for  $n_b \gtrsim n_0$ ,  $\beta$ -equilibrated matter is very neutron rich,  $\delta_{\text{eq}} \sim 1$ .

In addition to nuclear constraints, astrophysical NS properties provide useful insights on the EOS. Constraints derived from the observation of massive, isolated NS [14–20], from GW signals [21, 22] and multimessenger observations of binary neutron star (BNS) mergers [23–28], or by their combination [29, 30], are very informative about the high density regime. A key phenomenon in this respect is the prompt collapse (PC) to black hole (BH) of the merger remnant, since this behavior can influence both the GW and electromagnetic (EM) signals produced by BNS mergers [12, 16, 19, 31, 32, 34]. The PC behavior of equal mass BNSs was extensively explored in Ref. [20, 33, 37, 38, 40, 41, 58]. It was shown, for example, that the threshold mass for PC,  $M_{\text{th}}$ , normalized to  $M_{\max}^{\text{TOV}}$ , linearly correlates with the maximum compactness, defined as  $C_{\max}^{\text{TOV}} \equiv GM_{\max}^{\text{TOV}}/(R_{\max}^{\text{TOV}}c^2)$ , where  $c$  and  $G$  are the speed of light and the gravitational constant, respectively, as well as with other NS equilibrium properties. More recently, also the study of asymmetric BNS mergers has received attention [20, 59–61]. Bauswein *et al.* [20, 59] concluded that PC in asymmetric BNS usually occurs for masses equal or smaller than in the equal mass case, with the possible exception of modest asymmetries and very soft EOSs. The total mass reduc-

tion is stronger for more extreme mass ratios and it has a non-trivial dependence on the NS EOS. Tootle *et al.* [60] suggested instead a quasi-universal relation. In all these works, several fitting formulae to numerical results were provided.

In this *Letter*, we show that  $K_{\max}$ , the incompressibility of nuclear,  $\beta$ -equilibrated matter at  $n_{\max}^{\text{TOV}}$ , determines the behavior of BNS mergers close to PC and, in particular, their dependence on the mass ratio. Our results stem from the largest set of numerical relativity simulations of irrotational, asymmetric binaries with finite temperature, composition dependent microphysical EOSs to date. We demonstrate that the detection of  $M_{\text{th}}$  at two different mass ratios can provide a direct measurement of  $K_{\max}$  in a regime otherwise inaccessible. Additionally, we suggest that its value can yield information about the relevant thermodynamics degrees of freedom close to  $n_{\max}^{\text{TOV}}$ .

*Methods and models.-* We simulate 250 irrotational BNS mergers with different gravitational masses  $M \equiv M_1 + M_2 \in [2.786M_{\odot}, 3.3M_{\odot}]$  and mass ratios  $q \equiv M_1/M_2 \in \{0.6, 0.65, 0.7, 0.75, 0.85, 1\}$ . We perform series of simulations at fixed  $q$  while changing  $M$  to explore the onset of the PC behavior and determine  $M_{\text{th}}(q)$ . For the definition of  $M_{\text{th}}(q)$  and its numerical error,  $\delta M_{\text{th}}(q)$ , we follow Refs. [20, 33, 47], monitoring the maximum of the rest mass density,  $n_{\max}$ , throughout the computational domain. Simulations are performed with the same codes and setup as in Ref. [33];  $q = 1$  data are from Ref. [33], while  $q \neq 1$  data are presented here for the first time. See the Supplemental Material for more details.

To span present uncertainties, we consider six finite-temperature, composition dependent NS EOSs. Four are purely nucleonic and widely used: BL [24, 25], SFHo [50] and HS(DD2) [30, 55, hereafter DD2], and LS220 [42]. Additionally, we consider an EOS including hyperons, HS(BHB $\Lambda\phi$ ) [23, hereafter BHB], and one including a phase transition to quark matter, DD2qG, also presented in Ref. [33]. In both cases, the nucleonic baseline is DD2. In Figure 1, we present the nuclear incompressibility of neutrinoless,  $\beta$ -equilibrated, cold NS matter,  $K_{\text{eq}}$ , defined as in Eq. (1) but for  $\delta = \delta_{\text{eq}}$ , for the six different EOSs above as a function of  $n_b$ . For each EOS we highlight  $K_{\max} \equiv K(n_{\max}^{\text{TOV}})$ . It is striking that the properties in the low density regime ( $n_b < 2n_0$ ) do not necessarily correlate with those at  $n_b \sim n_{\max}^{\text{TOV}}$ . Moreover, the BL, SFHo and LS220 EOSs, despite being softer than the DD2 EOS, reach larger  $n_{\max}^{\text{TOV}}$  and provide similar, if not larger,  $K_{\max}$ .

*Results.-* Our simulations robustly indicate that PC occurs as  $n_{\max}$  approaches  $n_{\max}^{\text{TOV}}$  at merger. With the exception of the DD2qG EOS, for which  $n_{\max} \sim 0.8 - 1.2n_{\max}^{\text{TOV}}$ , for the heaviest non-PC BNS we observe  $n_{\max} \sim 0.75 - 0.95n_{\max}^{\text{TOV}}$  at the first remnant bounce, with larger values usually associated to  $q \sim 1$ .

Two opposite effects influence the evolution of  $n_{\max}$

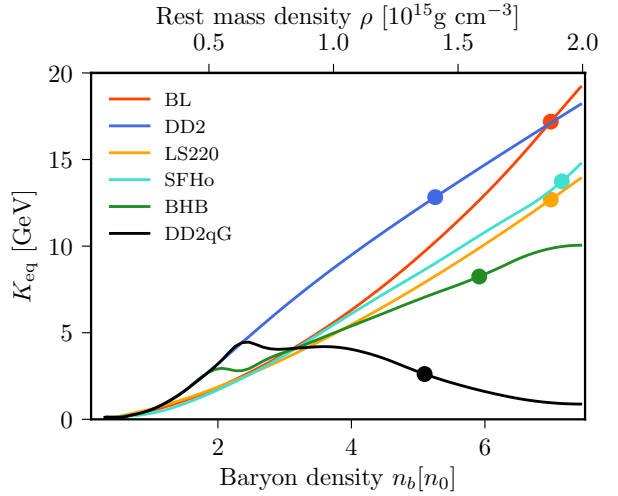


FIG. 1. Nuclear incompressibility  $K_{\text{eq}}$  of cold,  $\beta$ -equilibrated nuclear matter as a function of baryon density for the EOSs employed in this work. Solid markers correspond to  $K_{\max}$ , i.e.  $K_{\text{eq}}$  at the central density of the heaviest, irrotational NS.

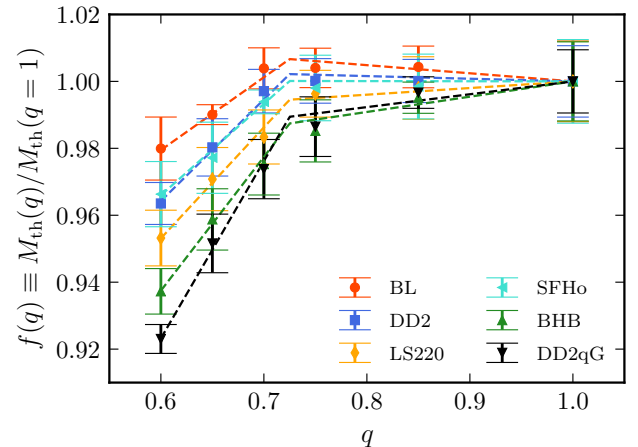


FIG. 2. Threshold PC masses normalized to the  $q = 1$  case as a function of  $q$  for all the EOS used in this work. Dashed lines correspond to Eq. (2) fit.

with respect to  $q$ . On the one hand, for a given  $M$ , binaries with smaller  $q$ 's have smaller orbital angular momentum and the NS cores are more prone to fuse (and thus to increase  $n_{\max}$  toward  $n_{\max}^{\text{TOV}}$ ) due to the smaller rotational support [20, 59]. On the other hand, the nuclear incompressibility usually increases as  $n_{\max}$  grows, providing a larger nuclear repulsion that contrasts its further increase. Since PC is observed for  $n_{\max} \sim n_{\max}^{\text{TOV}}$ , it is understandable that  $K_{\max}$  is the incompressibility value relevant for the PC behavior.

To analyse the dependence of PC on  $K_{\max}$ , in Figure 2 we first consider  $f(q) \equiv M_{\text{th}}(q)/M_{\text{th}}(q = 1)$  for

all EOSs, where (to be conservative) the error bars have been obtained by propagating the errors both on  $M_{\text{th}}(q)$  and  $M_{\text{th}}(q = 1)$ . Values of  $M_{\text{th}}$  and  $\delta M_{\text{th}}$  are reported in the Supplemental Material. We first observe that our results do not have a universal behavior for the different EOSs. Second, we notice that a variation of almost a factor of 1.7 in  $q$  has a small effect on  $M_{\text{th}}(q)$ , with the corresponding variation in  $f(q)$  ranging between 3% and 8%, larger for EOSs with a smaller  $K_{\text{max}}$ . This is broadly compatible to what observed in [20, 59–61] and should be compared with the larger ( $\lesssim 20\%$ ) variation in  $M_{\text{max}}^{\text{TOV}}$  or  $M_{\text{th}}(q = 1)/M_{\text{max}}^{\text{TOV}}$  reported in Refs. [20, 33, 34, 38, 40, 41, 47].

Focusing on the behavior of  $f(q)$  for  $0.7 \lesssim q \leq 1$  we observe that, depending on the EOS,  $f(q)$  can decrease, stay approximately constant or even increase as  $q$  decreases [see also 55, 59, 61]. We interpret this as the result of the interplay between the binary orbital angular momentum and the incompressibility of nuclear matter, in light of the merger dynamics. For BNSs with  $q \lesssim 1$  and  $M \approx M_{\text{th}}$ , the central density inside the more massive NS ranges in 0.40–0.49  $n_{\text{max}}$  (depending on the EOS) and the merger is driven by the fusion of two comparable NS cores. If  $K_{\text{eq}}$  increases steeply enough with  $n_{\text{max}}$ , nuclear repulsion contrasts efficiently gravity-driven compression. The net result is that for EOSs with a relatively large  $K_{\text{max}}$  (as BL, SFHo and DD2),  $M_{\text{th}}(q \lesssim 1)$  can stay rather constant or even increase as  $q$  decreases. On the opposite, if  $K_{\text{eq}}$  does not increase significantly with  $n_b$  and  $K_{\text{max}}$  is relatively low (as for DD2qG and BHB), nuclear repulsion is not enough to counterbalance the lack of rotational support and PC occurs for  $M_{\text{th}}(q \lesssim 1) < M_{\text{th}}(q = 1)$ .

Moving to  $0.6 \lesssim q \lesssim 0.7$ , we notice a clear change of behavior:  $f(q)$  decreases as  $q$  decreases for all EOSs. But, once again, the variation depends sensitively on  $K_{\text{max}}$ : EOSs characterized by a smaller  $K_{\text{max}}$  result not only in smaller  $f(q)$ , but also in larger relative variations with respect to  $f(q \approx 0.7)$ . We explain this transition in terms of the different merger dynamics. For BNSs at the PC threshold and with  $q \lesssim 0.7$ , the central density inside the more massive NS increases to 0.5–0.57  $n_{\text{max}}^{\text{TOV}}$ , while the secondary NS is more significantly deformed and tidally disrupted during the last orbits. As  $q$  decreases, the denser core of the more massive NS is compressed by more massive streams of accreting matter [16–20]. The nuclear incompressibility still opposes compression, but less efficiently than in the  $0.7 \lesssim q \leq 1$  regime.  $K_{\text{max}}$  still provides a measure of the NS matter resistance to compression in the relevant density interval and different EOSs result in different relative variations.

Our data qualitatively agree with those from independent simulations recently reported in Refs. [41, 60, 61]. However, quantitative differences comparable to the overall variation observed in our results are found. This is possibly due to different definitions of PC threshold, gravity treatment or numerical resolutions. A compari-

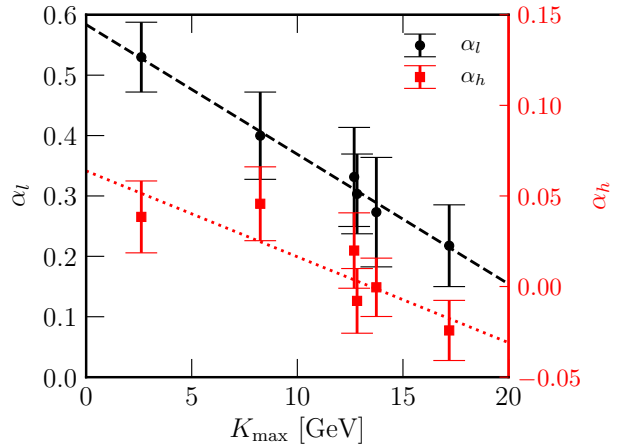


FIG. 3. Slopes of the fitting coefficients  $\alpha_{l,h}$  for data in Figure 2 as a function of  $K_{\text{max}}$ . Both slopes show a trend with  $K_{\text{max}}$  that we fitted with a linear function (dashed lines).

son with the some of the available fits is reported in the Supplemental Material. Moreover, our extended set of EOS indicates a sub-leading but significant and systematic EOS dependence emerging for asymmetric binaries, in contrast to a quasi-universal behavior [60].

Figure 2 suggests the existence of two different regimes, separated by  $0.7 \lesssim \tilde{q} \lesssim 0.75$ , which is largely independent from the EOS. In each of the two regimes,  $f(q)$  is well described by a linear relation. Thus, for each EOS we fit our data by considering:

$$f(q) = \alpha(q)q + \beta(q) = \begin{cases} \alpha_l q + \beta_l & \text{if } q < \tilde{q}, \\ \alpha_h q + \beta_h & \text{if } q \geq \tilde{q}. \end{cases} \quad (2)$$

We fix  $\beta_{l,h}$  in Eq. (2) by imposing the continuity of  $f(q)$  at  $q = \tilde{q}$  and  $f(q = 1) = 1$ . Moreover, we assume  $\tilde{q} = 0.725$  by closely inspecting Figure 2. Least square fits (dashed lines) are performed on the two parameters  $\alpha_{l,h}$ , corresponding to the slopes of the two linear regimes. The residuals relative to the errors are always smaller than 0.5 and without clear systematic trends both with respect to the EOS and  $q$ .

Our simulations reveal a correlation between  $\alpha_{l,h}$  and  $K_{\text{max}}$  supporting the interpretation that the latter is one of the key properties that control the PC. In Figure 3, we represent  $\alpha_{l,h}$  with their uncertainties as a function of  $K_{\text{max}}$  for each EOS. Given the reduced number of EOSs and the relatively large uncertainties, we fit  $\alpha_{l,h}$  with a first order polynomial in  $K_{\text{max}}$  (dashed lines in Figure 3):

$$\begin{aligned} \alpha_l &= -(22 \pm 1)\text{TeV}^{-1}K_{\text{max}} + (0.58 \pm 0.01), \\ \alpha_h &= -(4.7 \pm 1.0)\text{TeV}^{-1}K_{\text{max}} + (0.064 \pm 0.017). \end{aligned} \quad (3)$$

The slopes of the linear behaviors observed in Figure 2 usually decrease as the incompressibility increases. This

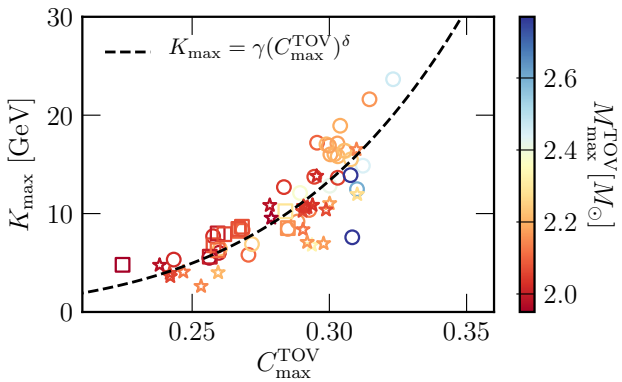


FIG. 4.  $K_{\max}$  as a function of the compactness of the heaviest NS for a large sample of EOSs. Circles correspond to nucleonic EOSs, while squares and stars to EOSs containing hyperons or undergoing a phase transition to quarks, respectively.

confirms that EOSs with a large incompressibility provide a possible increase in  $M_{\text{th}}$  for  $\tilde{q} < q \leq 1$  and a less steep decrease for  $q < \tilde{q}$ .

*Discussion.-* Our results suggest that the determination of  $M_{\text{th}}$  at two different  $q$ 's,  $q_{1,2}$ , allows to determine  $K_{\max}$  by solving:

$$\frac{M_{\text{th}}(q_1)}{M_{\text{th}}(q_2)} = \frac{\alpha(K_{\max}, q_1)q_1 + \beta(\alpha)}{\alpha(K_{\max}, q_2)q_2 + \beta(\alpha)}, \quad (4)$$

where  $\alpha$  and  $\beta$  are defined consistently with Eqs. (2) and (3). To test this, we repeat the previous fits excluding results from the SFHo EOS. The new fitted coefficients,  $\alpha'_{l,h}$ , are compatible to within uncertainties with  $\alpha_{l,h}$  in Eq. (3). We deduce  $K_{\max}$  for SFHo using these new fits and the  $M_{\text{th}}(q)$  SFHo results at two different  $q$ 's. In particular, we randomly sample the intervals  $(M_{\text{th}}(q) \pm \delta M_{\text{th}}(q)/2)$  one thousand times to set simulated values for the threshold masses,  $\tilde{M}_{\text{th}}(q_{1,2})$ , and to compute  $\tilde{K}_{\max}$  by solving Eq. (4). We finally extract the average relative discrepancy between the computed and actual values. For example, using  $M_{\text{th}}(q = 0.65)$  and  $M_{\text{th}}(q = 0.85)$  we recover  $K_{\max}$  to within 2% of its actual value. The uncertainty increases when considering  $M_{\text{th}}(q = 0.7)$  and  $M_{\text{th}}(q = 0.85)$ . In this case,  $K_{\max}$  is recovered to within 15%. Our method does not necessarily require the knowledge of  $M_{\text{th}}(q)$  at two  $q \neq 1$ . For example, using  $M_{\text{th}}(q = 0.7)$  and  $M_{\text{th}}(q = 1)$  we recover  $K_{\max}$  within 3.5%. The above discrepancies on  $K_{\max}$  are compatible with the uncertainties implied by Figure 3.

To further challenge our method, we consider the independent results for  $M_{\text{th}}(q)$  from Ref. [60] obtained for irrotational NSs and for the TNTYST EOS [58], an EOS not included in our sample and for which  $K_{\max} > 20\text{GeV}$

<sup>1</sup>. We consider the  $\alpha_{l,h}$  fits, Eq. (3), and we solve Eqs. (4) and (5) using  $M_{\text{th}}(q = 0.7)$  and  $M_{\text{th}}(q = 0.9)$ . Despite possible systematical differences related to the different way to determine  $M_{\text{th}}$ , we recover the expected value of  $K_{\max}$  to within 25% ( $\sim 6\text{ GeV}$ ) of its actual value.

Prompted by these results, we investigate a direct correlation between  $C_{\max}^{\text{TOV}}$  and  $K_{\max}$  and we find that the values of  $K_{\max}$  can provide information on the relevant degrees of freedom in ultradense matter. In Figure 4, we present  $K_{\max}$  as a function of  $C_{\max}^{\text{TOV}}$  for a large set of EOSs. In particular, we selected EOSs that stay causal up to  $n_{\max}^{\text{TOV}}$  and for which  $M_{\max}^{\text{TOV}} > 1.97M_{\odot}$ . More detailed information can be found in the Supplemental Material. Different symbols refer to different particle contents while colors to  $M_{\max}^{\text{TOV}}$ . We suggest that large  $K_{\max} (\gtrsim 15\text{ GeV})$  are more easily associated with purely nucleonic EOSs, while EOSs containing hyperons or showing a phase transition to quarks are characterized by small  $K_{\max} (\lesssim 15\text{ GeV})$ . A tighter threshold at  $12\text{ GeV}$  can be observed if only two EOSs containing just  $u$  and  $d$  quarks, out a sample of 34 EOSs containing quarks or hyperons, were removed. Moreover,  $K_{\max}$  can be fitted in good approximation with a power law,  $K_{\max} = \gamma(C_{\max}^{\text{TOV}})^{\delta}$ . Standard least squared methods provide  $\gamma = (9.2 \pm 5.4)\text{TeV}$  and  $\delta = 5.67 \pm 0.50$ . Despite not being trivial, such a relation is not surprising, since both  $M_{\max}^{\text{TOV}}$  and  $R_{\max}^{\text{TOV}}$  depend on the equilibrium response of the heaviest NS to radial perturbations for  $n_b \sim n_{\max}^{\text{TOV}}$ , and thus on  $K_{\max}$ . Moreover, it provides a possible connection between our findings and previous, different fits for  $M_{\text{th}}$  expressed in terms of  $M_{\max}^{\text{TOV}}$  and  $C_{\max}^{\text{TOV}}$ , both for symmetric and asymmetric mergers [20, 33, 40, 58, 59, 61]. For example, we have repeated our analysis in terms of  $C_{\max}^{\text{TOV}}$  rather than  $K_{\max}$ , finding comparable results, as reported in the Supplemental Material. Even if this relation directly connects  $K_{\max}$  to  $C_{\max}^{\text{TOV}}$ , we stress that  $K_{\max}$  provides a cleaner and more intuitive physical interpretation of the PC behavior for  $q \neq 1$ .

This  $K_{\max}(C_{\max}^{\text{TOV}})$  relation, combined with the linear relation  $M_{\text{th}}(q = 1)/M_{\max}^{\text{TOV}} = aC_{\max}^{\text{TOV}} + b$  first proposed in Ref. [58] but with coefficients from Ref. [33], suggests that  $M_{\max}^{\text{TOV}}$  can be also related to  $K_{\max}$  and  $M_{\text{th}}(q = 1)$ :

$$M_{\max}^{\text{TOV}} = \frac{M_{\text{th}}(q = 1)}{a(K_{\max}/\gamma)^{1/\delta} + b}. \quad (5)$$

Eqs. (2) and (5) together suggest that  $K_{\max}$  can be estimated by the knowledge of only one  $M_{\text{th}}(q)$ , if  $M_{\max}^{\text{TOV}}$  is known:

$$\frac{M_{\text{th}}(q)}{M_{\max}^{\text{TOV}}(a(K_{\max}/\gamma)^{1/\delta} + b)} = \alpha(K_{\max}, q)q + \beta(\alpha). \quad (6)$$

<sup>1</sup> We notice, however, that the TNTYST EOS becomes acausal close to  $n_{\max}^{\text{TOV}}$ .

For example, using the  $\alpha'_{l,h}$  fits while employing  $M_{\max}^{\text{TOV}}$  and  $M_{\text{th}}(q = 0.85)$  SFHo results as input data, we recover  $K_{\max}$  and  $C_{\max}^{\text{TOV}}$  to within 40% and 1.6%, respectively. Comparable results were obtained from smaller  $q$ 's.

The analogy between the definition of  $K_{\text{eq}}$  and the square of the speed of sound of NS matter,  $c_s^2 = \partial P / \partial \epsilon|_{T=0,\delta_{\text{eq}}}$ , where  $\epsilon$  is the density of internal energy, suggests that the measurement of the PC threshold at different  $q$ 's can also provide constraints on the value of  $c_s^2$  close to  $n_{\max}^{\text{TOV}}$ . Indeed, the  $\alpha$  and  $\beta$  coefficients of Eq. (2) also correlate with  $c_s^2$  in a comparable way as with  $K_{\max}$  and  $C_{\max}^{\text{TOV}}$ , as visible in the Supplemental Material. Constraints on  $c_s$  can provide further insight into the physics governing the EOS of nuclear matter [see e.g. 60, 61].

The larger detection horizon associated to massive BNS mergers suggests that, as in the case of GW190425 [62], PCs are a viable observational phenomenon associated to a significant fraction of BNSs that will become accessible in the next GW observing runs [63, 64] and with 3rd generation GW detectors [65–67]. While current GW detections allow the precise measurement of the chirp mass and, up to a certain extent, of the total mass, the mass ratio is more uncertain. High enough signal-to-noise ratios and good sky localizations favoring followup EM observations will be key to provide better constraints on  $q$ . We estimate the possible impact of the uncertainties on  $M_{\text{th}}$  and on  $q$  on the estimate of  $K_{\max}$  by solving again Eq. (4), using the  $\alpha'_{l,h}$  fitted coefficients (i.e. considering SFHo as our underlying EOS and removing it from our fitting sample). We randomly sample both  $M_{\text{th}}$  and  $q$  within  $M_{\text{th}} \pm \Delta M_{\text{th}}$  and  $q \pm \Delta q$ , where  $\Delta M_{\text{th}}$  and  $\Delta q$  are the uncertainties in the determination of  $M_{\text{th}}(q)$ . In the case of  $q = 0.85$  and  $q = 0.65$ , to determine  $K_{\max}$  with at least 30% accuracy at 90% confidence level we estimate  $\Delta M_{\text{th}} \lesssim 0.025M_{\odot}$  and  $\Delta q \lesssim 0.05$ . For  $q = 0.85$  and  $q = 0.70$ , the uncertainties should decrease to  $\Delta M_{\text{th}} \lesssim 0.01M_{\odot}$  and  $\Delta q \lesssim 0.025$  to get a similar accuracy. The difference between the two cases proves that, due to the larger slope of  $M_{\text{th}}(q)$  at  $q \ll 1$ , the determination of  $M_{\text{th}}(q)$  for very asymmetric systems is more constraining. Such uncertainties are within reach of future observations and detectors [68].

More theoretical PC studies will be needed to reduce systematic uncertainties and include more detailed physics. Nevertheless, our results clearly indicate a new and unique way to access critical information on extreme density nuclear physics using observations of promptly collapsing BNS mergers.

*Acknowledgments.*— A.Pe. thanks Matteo Breschi for useful discussions. A.Pe., D.L. and S.B. acknowledge the INFN for the usage of computing and storage resources through the *tullio* cluster in Turin. The authors acknowledge the usage of EOS tables from the CompOSE website, <https://compose.obspm.fr>. D.L. thanks also C. Providencia for providing some EOS tables. A.Pe. and D.L. acknowledge PRACE for

awarding them access to Joliot-Curie at GENCI@CEA. A.Pe. also acknowledges the usage of computer resources under a CINECA-INFN agreement (allocation INF20\_teongrav and INF21\_teongrav). S.B. acknowledges funding from the EU H2020 under ERC Starting Grant, no.BinGraSp-714626, and from the Deutsche Forschungsgemeinschaft, DFG, project MEMI number BE 6301/2-1. D.R. acknowledges funding from the U.S. Department of Energy, Office of Science, Division of Nuclear Physics under Award Number(s) DE-SC0021177 and from the National Science Foundation under Grants No. PHY-2011725, PHY-2020275, PHY-2116686, and AST-2108467. NR simulations were performed on Joliot-Curie at GENCI@CEA (PRACE-ra5202), SuperMUC-LRZ (Gauss project pn56zo), Marconi-CINECA (ISCRA-B project HP10BMHFQQ, INF20\_teongrav and INF21\_teongrav allocation); Bridges, Comet, Stampede2 (NSF XSEDE allocation TG-PHY160025), NSF/NCSA Blue Waters (NSF AWD-1811236), supercomputers. This research used resources of the National Energy Research Scientific Computing Center, a DOE Office of Science User Facility supported by the Office of Science of the U.S. Department of Energy under Contract No. DE-AC02-05CH11231.

- 
- [1] J. M. Lattimer and M. Prakash, Phys. Rept. **621**, 127 (2016), arXiv:1512.07820 [astro-ph.SR].
  - [2] M. Oertel, M. Hempel, T. Klähn, and S. Typel, Rev. Mod. Phys. **89**, 015007 (2017), arXiv:1610.03361 [astro-ph.HE].
  - [3] R. Machleidt and D. R. Entem, Phys. Rept. **503**, 1 (2011), arXiv:1105.2919 [nucl-th].
  - [4] D. Chatterjee and I. Vidaña, Eur. Phys. J. A **52**, 29 (2016), arXiv:1510.06306 [nucl-th].
  - [5] D. Logoteta, Universe **7**, 408 (2021).
  - [6] I. Bombaci, D. Logoteta, I. Vidaña, and C. Providência, Eur. Phys. J. A **52**, 58 (2016), arXiv:1601.04559 [astro-ph.HE].
  - [7] P. Braun-Munzinger and J. Wambach, Reviews of Modern Physics **81**, 1031 (2009).
  - [8] S. Benic, D. Blaschke, D. E. Alvarez-Castillo, T. Fischer, and S. Typel, Astron. Astrophys. **577**, A40 (2015), arXiv:1411.2856 [astro-ph.HE].
  - [9] U. Garg and G. Colò, Prog. Part. Nucl. Phys. **101**, 55 (2018), arXiv:1801.03672 [nucl-ex].
  - [10] S. Shlomo, V. M. Kolomietz, and G. Colò, European Physical Journal A **30**, 23 (2006).
  - [11] D. H. Youngblood, H. L. Clark, and Y. W. Lui, Phys. Rev. Lett. **82**, 691 (1999).
  - [12] J. R. Stone, N. J. Stone, and S. A. Moszkowski, Phys. Rev. C **89**, 044316 (2014), arXiv:1404.0744 [nucl-th].
  - [13] P. Avogadro and C. A. Bertulani, Phys. Rev. C **88**, 044319 (2013), arXiv:1305.7299 [nucl-th].
  - [14] P. Demorest, T. Pennucci, S. Ransom, M. Roberts, and J. Hessels, Nature **467**, 1081 (2010), arXiv:1010.5788 [astro-ph.HE].
  - [15] J. Antoniadis, P. C. Freire, N. Wex, T. M. Tauris, R. S.

- Lynch, *et al.*, Science **340**, 6131 (2013), arXiv:1304.6875 [astro-ph.HE].
- [16] H. T. Cromartie *et al.* (NANOGrav), Nature Astron. **4**, 72 (2019), arXiv:1904.06759 [astro-ph.HE].
- [17] E. Fonseca *et al.*, Astrophys. J. Lett. **915**, L12 (2021), arXiv:2104.00880 [astro-ph.HE].
- [18] M. C. Miller *et al.*, Astrophys. J. Lett. **918**, L28 (2021), arXiv:2105.06979 [astro-ph.HE].
- [19] T. E. Riley *et al.*, Astrophys. J. Lett. **918**, L27 (2021), arXiv:2105.06980 [astro-ph.HE].
- [20] N.-B. Zhang and B.-A. Li, Astrophys. J. **921**, 111 (2021), arXiv:2105.11031 [nucl-th].
- [21] B. P. Abbott *et al.* (LIGO Scientific, Virgo), Phys. Rev. Lett. **121**, 161101 (2018), arXiv:1805.11581 [gr-qc].
- [22] S. De, D. Finstad, J. M. Lattimer, D. A. Brown, E. Berger, and C. M. Biwer, Phys. Rev. Lett. **121**, 091102 (2018), [Erratum: Phys. Rev. Lett. 121,no.25,259902(2018)], arXiv:1804.08583 [astro-ph.HE].
- [23] D. Radice, A. Perego, F. Zappa, and S. Bernuzzi, Astrophys. J. **852**, L29 (2018), arXiv:1711.03647 [astro-ph.HE].
- [24] D. Radice and L. Dai, Eur. Phys. J. **A55**, 50 (2019), arXiv:1810.12917 [astro-ph.HE].
- [25] A. Bauswein, O. Just, H.-T. Janka, and N. Stergioulas, Astrophys. J. **850**, L34 (2017), arXiv:1710.06843 [astro-ph.HE].
- [26] B. Margalit and B. D. Metzger, Astrophys. J. **850**, L19 (2017), arXiv:1710.05938 [astro-ph.HE].
- [27] E. R. Most, L. R. Weih, L. Rezzolla, and J. Schaffner-Bielich, Phys. Rev. Lett. **120**, 261103 (2018), arXiv:1803.00549 [gr-qc].
- [28] M. Breschi, A. Perego, S. Bernuzzi, W. Del Pozzo, V. Nedora, D. Radice, and D. Vescovi, Mon. Not. Roy. Astron. Soc. **505**, 1661 (2021), arXiv:2101.01201 [astro-ph.HE].
- [29] G. Raaijmakers, S. K. Greif, K. Hebeler, T. Hinderer, S. Nissanke, A. Schwenk, T. E. Riley, A. L. Watts, J. M. Lattimer, and W. C. G. Ho, Astrophys. J. Lett. **918**, L29 (2021), arXiv:2105.06981 [astro-ph.HE].
- [30] P. T. H. Pang, I. Tews, M. W. Coughlin, M. Bulla, C. Van Den Broeck, and T. Dietrich, Astrophys. J. **922**, 14 (2021), arXiv:2105.08688 [astro-ph.HE].
- [31] K. Hotokezaka, K. Kiuchi, K. Kyutoku, H. Okawa, Y.-i. Sekiguchi, *et al.*, Phys. Rev. **D87**, 024001 (2013), arXiv:1212.0905 [astro-ph.HE].
- [32] K. Hotokezaka, K. Kiuchi, K. Kyutoku, T. Muranushi, Y.-i. Sekiguchi, *et al.*, Phys. Rev. **D88**, 044026 (2013), arXiv:1307.5888 [astro-ph.HE].
- [33] A. Bauswein, S. Goriely, and H.-T. Janka, Astrophys. J. **773**, 78 (2013), arXiv:1302.6530 [astro-ph.SR].
- [34] M. Agathos, F. Zappa, S. Bernuzzi, A. Perego, M. Breschi, and D. Radice, Phys. Rev. **D101**, 044006 (2020), arXiv:1908.05442 [gr-qc].
- [35] D. Radice, A. Perego, K. Hotokezaka, S. A. Fromm, S. Bernuzzi, and L. F. Roberts, Astrophys. J. **869**, 130 (2018), arXiv:1809.11161 [astro-ph.HE].
- [36] S. Bernuzzi *et al.*, Mon. Not. Roy. Astron. Soc. (2020), 10.1093/mnras/staa1860, arXiv:2003.06015 [astro-ph.HE].
- [37] M. Shibata, K. Taniguchi, and K. Uryu, Phys. Rev. **D71**, 084021 (2005), arXiv:gr-qc/0503119.
- [38] K. Hotokezaka, K. Kyutoku, H. Okawa, M. Shibata, and K. Kiuchi, Phys. Rev. **D83**, 124008 (2011), arXiv:1105.4370 [astro-ph.HE].
- [39] A. Bauswein, T. Baumgarte, and H. T. Janka, Phys. Rev. Lett. **111**, 131101 (2013), arXiv:1307.5191 [astro-ph.SR].
- [40] S. Köppel, L. Bovard, and L. Rezzolla, Astrophys. J. **872**, L16 (2019), arXiv:1901.09977 [gr-qc].
- [41] A. Bauswein and N. Stergioulas, J. Phys. G **46**, 113002 (2019), arXiv:1901.06969 [gr-qc].
- [42] A. Bauswein, S. Blacker, V. Vijayan, N. Stergioulas, K. Chatzioannou, J. A. Clark, N.-U. F. Bastian, D. B. Blaschke, M. Cierniak, and T. Fischer, Phys. Rev. Lett. **125**, 141103 (2020), arXiv:2004.00846 [astro-ph.HE].
- [43] R. Kashyap *et al.*, (2021), arXiv:2111.05183 [astro-ph.HE].
- [44] A. Bauswein, S. Blacker, G. Lioutas, T. Soulantasis, V. Vijayan, and N. Stergioulas, Phys. Rev. D **103**, 123004 (2021), arXiv:2010.04461 [astro-ph.HE].
- [45] S. D. Tootle, L. J. Papenfort, E. R. Most, and L. Rezzolla, (2021), arXiv:2109.00940 [gr-qc].
- [46] M. Kölsch, T. Dietrich, M. Ujevic, and B. Bruegmann, (2021), arXiv:2112.11851 [gr-qc].
- [47] A. Bauswein, H. Janka, K. Hebeler, and A. Schwenk, Phys. Rev. **D86**, 063001 (2012), arXiv:1204.1888 [astro-ph.SR].
- [48] I. Bombaci and D. Logoteta, Astron. Astrophys. **609**, A128 (2018), arXiv:1805.11846 [astro-ph.HE].
- [49] D. Logoteta, A. Perego, and I. Bombaci, (2020), 10.1051/0004-6361/202039457, arXiv:2012.03599 [nucl-th].
- [50] A. W. Steiner, M. Hempel, and T. Fischer, Astrophys. J. **774**, 17 (2013), arXiv:1207.2184 [astro-ph.SR].
- [51] S. Typel, G. Ropke, T. Klähn, D. Blaschke, and H. H. Wolter, Phys. Rev. **C81**, 015803 (2010), arXiv:0908.2344 [nucl-th].
- [52] M. Hempel and J. Schaffner-Bielich, Nucl. Phys. **A837**, 210 (2010), arXiv:0911.4073 [nucl-th].
- [53] J. M. Lattimer and F. D. Swesty, Nucl. Phys. **A535**, 331 (1991).
- [54] S. Banik, M. Hempel, and D. Bandyopadhyay, Astrophys. J. Suppl. **214**, 22 (2014), arXiv:1404.6173 [astro-ph.HE].
- [55] K. Kiuchi, K. Kyohei, K. Kyutoku, Y. Sekiguchi, and M. Shibata, (2019), arXiv:1907.03790 [astro-ph.HE].
- [56] T. Dietrich, N. Moldenhauer, N. K. Johnson-McDaniel, S. Bernuzzi, C. M. Markakis, B. Brügmann, and W. Tichy, Phys. Rev. **D92**, 124007 (2015), arXiv:1507.07100 [gr-qc].
- [57] T. Dietrich, M. Ujevic, W. Tichy, S. Bernuzzi, and B. Brügmann, Phys. Rev. **D95**, 024029 (2017), arXiv:1607.06636 [gr-qc].
- [58] H. Togashi, K. Nakazato, Y. Takehara, S. Yamamuro, H. Suzuki, and M. Takano, Nucl. Phys. A **961**, 78 (2017), arXiv:1702.05324 [nucl-th].
- [59] N.-U. F. Bastian, Phys. Rev. D **103**, 023001 (2021), arXiv:2009.10846 [nucl-th].
- [60] I. Tews, J. Carlson, S. Gandolfi, and S. Reddy, Astrophys. J. **860**, 149 (2018), arXiv:1801.01923 [nucl-th].
- [61] C. D. Capano, I. Tews, S. M. Brown, B. Margalit, S. De, S. Kumar, D. A. Brown, B. Krishnan, and S. Reddy, Nature Astron. **4**, 625 (2020), arXiv:1908.10352 [astro-ph.HE].
- [62] B. Abbott *et al.* (LIGO Scientific, Virgo), Astrophys. J. Lett. **892**, L3 (2020), arXiv:2001.01761 [astro-ph.HE].
- [63] B. P. Abbott *et al.* (VIRGO, KAGRA, LIGO Scientific), Living Rev. Rel. **21**, 3 (2018), [Living Rev.

- Rel.19,1(2016)], arXiv:1304.0670 [gr-qc].
- [64] B. P. Abbott *et al.* (KAGRA, LIGO Scientific, Virgo, VIRGO), Living Rev. Rel. **21**, 3 (2018), arXiv:1304.0670 [gr-qc].
- [65] M. Punturo, M. Abernathy, F. Acernese, B. Allen, N. Andersson, *et al.*, Class.Quant.Grav. **27**, 194002 (2010).
- [66] M. Maggiore *et al.*, JCAP **03**, 050 (2020), arXiv:1912.02622 [astro-ph.CO].
- [67] D. Reitze, R. X. Adhikari, S. Ballmer, B. Barish, L. Barsotti, G. Billingsley, D. A. Brown, Y. Chen, D. Coyne, R. Eisenstein, M. Evans, P. Fritschel, E. D. Hall, A. Lazzarini, G. Lovelace, J. Read, B. S. Sathyaprakash, D. Shoemaker, J. Smith, C. Torrie, S. Vitale, R. Weiss, C. Wipf, and M. Zucker, in *Bulletin of the American Astronomical Society*, Vol. 51 (2019) p. 35, arXiv:1907.04833 [astro-ph.IM].
- [68] S. Borhanian and B. S. Sathyaprakash, (2022), arXiv:2202.11048 [gr-qc].

## SUPPLEMENTAL MATERIAL

### Simulation sample

We evolve our BNSs using the publicly available **WhiskyTHC** code [1–3], built on the top of the **EinsteinToolkit** [4]. **WhiskyTHC** solves general relativistic hydrodynamics in conservative form using high-resolution shock-capturing finite-volume schemes based on high-order reconstruction operators. The spacetime metric is evolved in the Z4c formulation of Einstein’s equations [5, 6] implemented by the **CTGamma** module [7, 8] of **EinsteinToolkit**.

To properly resolve the merger dynamics, we employ an adaptive mesh refinement consisting in seven nested grids with 1:2 linear scaling between consecutive grids and provided by the **Carpet** library [9]. The latter implements the Berger-Oliger scheme with refluxing [10, 11]. The resolution of the innermost grid,  $h$ , characterizes each simulation and we distinguish between low ( $h \approx 246$  m, LR), standard ( $h \approx 185$  m, SR) and high ( $h \approx 123$  m, HR) resolutions. More details on the grid setup were discussed in detail in Ref. [12]. All simulations were performed with microphysical EOS, also accounting for neutrino emission using the leakage scheme discussed in [13, 14].

Initial conditions are obtained by the pseudospectral elliptic solver **Lorene** [15]. The initial separation between the centers of the two stars is typically taken to be 40 km.

All configuration immediately above or below  $M_{\text{th}}$  were run at least at two resolutions (LR and SR). For a few selected cases we performed also HR runs. In total, we performed 250 BNS merger simulations: 125 at LR, 116 at SR and 9 at HR. The PC threshold and its error have been computed using the two highest available resolutions. Thus the error bars include numerical resolution uncertainty. A summary of our results is reported in Table (I).

In Figure 5, we present the rest mass density on the orbital plane just after merger for a  $M \gtrsim M_{\text{th}}$  and for two SR simulations characterized by  $q = 0.85$  (left panel) and  $q = 0.65$  (right panel) to highlight quantitative differences. Tidal interaction and deformation is present in both cases, but with different features. In the  $q = 0.85$  case, the two NS cores are mostly preserved during the late inspiral and the subsequent remnant dynamics is governed by the core fusion process. This is visible in the left panel of Figure 5 where, opposite to the tidal tail produced by the tidal stripping of secondary NS, a larger amount of shocked matter is expelled as consequence of the collision of the two cores. As  $q$  decreases further below  $\tilde{q} = 0.725$ , the secondary NS is more significantly deformed during the last orbits and even its core gets affected. A significant accretion stream flows from the deformed core of the secondary toward the primary such that the debris of the secondary form an envelop that wraps the primary NS up [16–20]. This prominent change in the dynamics is visible in the right panel of Figure 5 where the tidal tail of the secondary is now much more relevant and the interaction between the two cores happens in form of an accretion stream rather than of the fusion of two comparable cores.

### Nuclear Incompressibility

In Table (II), we report some of the relevant properties of all the EOSs used to produce figure 4 of the main text. For each EOS, in addition to the name, we report the mass and the radius of the heaviest NS,  $M_{\text{max}}^{\text{TOV}}$ ,  $R_{\text{max}}^{\text{TOV}}$  respectively, its central density,  $n_{\text{max}}^{\text{TOV}}$ , and the incompressibility at  $n_{\text{max}}^{\text{TOV}}$ ,  $K_{\text{max}}$ . Overall, our sample consists of 66 cold, beta equilibrated EOSs. Among them, 12 include hyperons and 22 model a phase transition to quark matter.

### Alternative analysis and comparison with existing fits

As highlighted in the main text, the relation between  $C_{\text{max}}^{\text{TOV}}$  and  $K_{\text{max}}$  implied by figure 4 suggests the possibility of repeating the PC analysis in terms of a single variable, either  $C_{\text{max}}^{\text{TOV}}$  or  $K_{\text{max}}$ . We first consider the  $q = 1$  data presented in Ref. [33] for which the linear fit  $M_{\text{th}}(q = 1)/M_{\text{max}}^{\text{TOV}} = aC_{\text{max}}^{\text{TOV}} + b$  was proposed [see e.g. 58]. By inserting the ansatz  $K_{\text{max}} = \alpha(C_{\text{max}}^{\text{TOV}})^{1/\delta}$ , we obtain  $M_{\text{th}}(q = 1)/M_{\text{max}}^{\text{TOV}} = a'(K_{\text{max}}/1\text{GeV})^{d'} + b'$ . Standard least square methods yield to  $a' = (-4.3 \pm 3.5) \times 10^{-4}$ ,  $b' = 1.469 \pm 0.009$  and  $d' = 2.01 \pm 0.26$ . The points and the result of the fit are reported in the left panel of Figure 6. However, the fit in  $C_{\text{max}}^{\text{TOV}}$  should be preferred since it provides a tighter correlation and it uses one fitting parameter less.

TABLE I. Summary of the threshold masses and of their error of numerical origin, for each of the equations of state used in this work and for all the explored mass ratios.

EOS	$(M_{\text{th}} \pm \delta M_{\text{th}}) [M_{\odot}]$					
	$q = 0.6$	$q = 0.65$	$q = 0.7$	$q = 0.75$	$q = 0.85$	$q = 1.0$
BL	$2.865 \pm 0.019$	$2.895 \pm 0.006$	$2.935 \pm 0.012$	$2.936 \pm 0.012$	$2.937 \pm 0.012$	$2.924 \pm 0.024$
DD2	$3.155 \pm 0.014$	$3.210 \pm 0.020$	$3.264 \pm 0.015$	$3.275 \pm 0.015$	$3.274 \pm 0.014$	$3.274 \pm 0.024$
LS220	$2.817 \pm 0.017$	$2.870 \pm 0.020$	$2.907 \pm 0.017$	$2.945 \pm 0.014$	$2.950 \pm 0.019$	$2.956 \pm 0.025$
SFHo	$2.729 \pm 0.019$	$2.760 \pm 0.021$	$2.807 \pm 0.007$	$2.819 \pm 0.019$	$2.820 \pm 0.019$	$2.824 \pm 0.024$
BHB	$2.835 \pm 0.015$	$2.900 \pm 0.020$	$2.950 \pm 0.020$	$2.980 \pm 0.020$	$3.010 \pm 0.010$	$3.024 \pm 0.025$
DD2qG	$2.910 \pm 0.010$	$3.000 \pm 0.020$	$3.070 \pm 0.020$	$3.110 \pm 0.020$	$3.142 \pm 0.010$	$3.152 \pm 0.021$

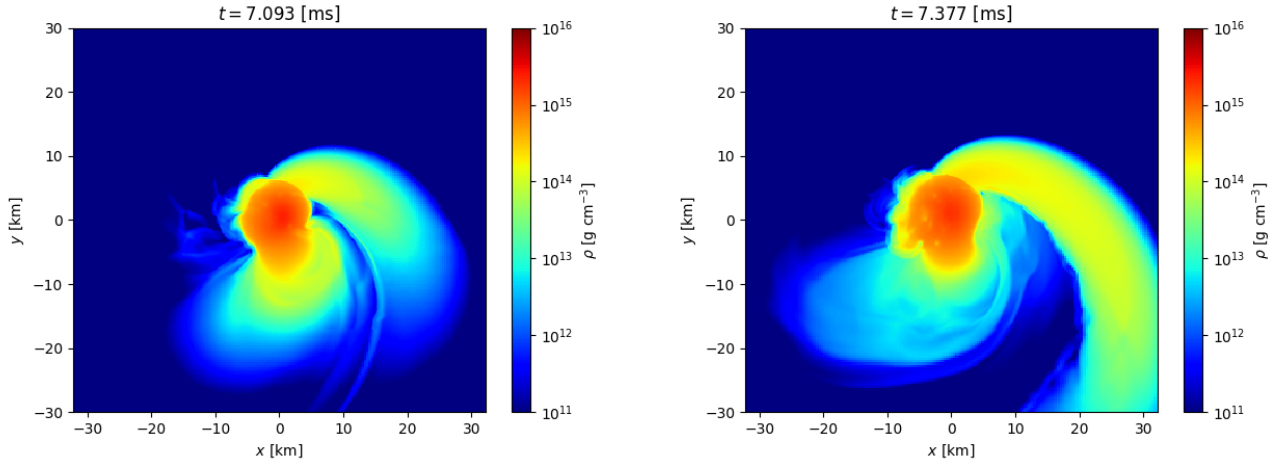


FIG. 5. Rest mass density in the orbital plane for two BNS merger simulations performed with the SFHo EOS, during the late inspiral phase and just prior to the prompt collapse of the remnant. The left panel refer to  $q = 0.85$ , while the right one to  $q = 0.65$ . In the former case, the tidal disruption of the secondary NS is marginal and the merger dynamics is driven by the core fusion, as testified by the ejection of shocked matter opposite to the tidal tail. In the latter case, the core of the secondary is significantly affected by tidal interaction and a large accretion stream flows onto the primary core.

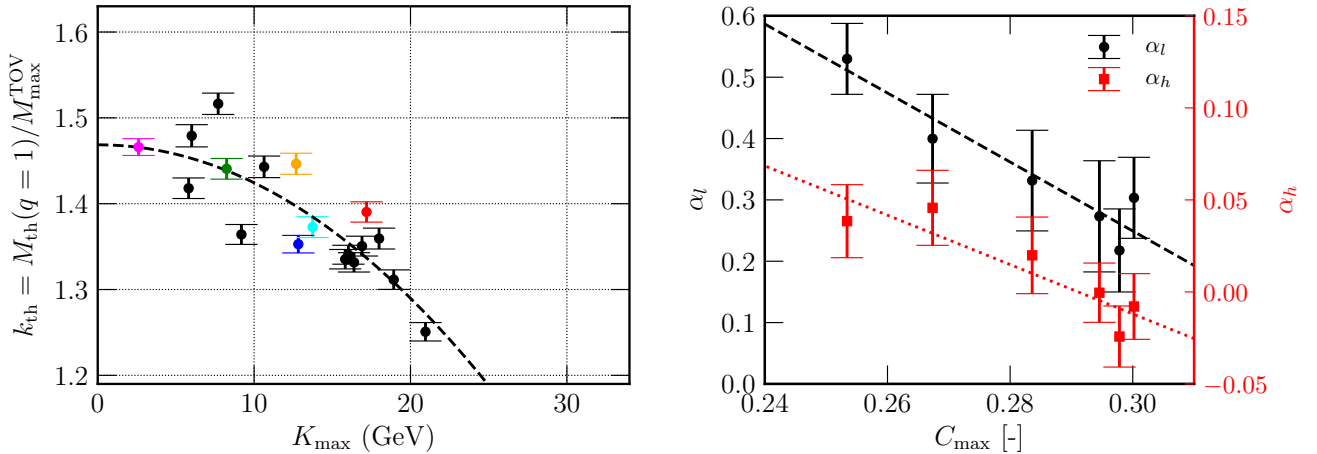


FIG. 6. Left:  $k_{\text{th}} \equiv M_{\text{th}}(q = 1)/M_{\text{max}}^{\text{TOV}}$  as a function of  $K_{\text{max}}$  from the  $q = 1$  results reported in [33], for the EOSs for which  $M_{\text{max}}^{\text{TOV}} > 1.97M_{\odot}$ . The dashed line correspond to the power-law fit described in the text. The colored points corresponds to the six EOSs used in this work. Right: Slope parameters,  $\alpha_{l,h}$ , presented in the main text (see equations 2 and 3), as a function of the maximum compactness,  $C_{\text{max}}$ . The dashed and dotted lines represent a linear fit with respect to  $C_{\text{max}}^{\text{TOV}}$ .

TABLE II. Incompressibility at the maximum central density for each of the equations of state used in Figure 5 of this work. For each equation of state, in addition to the name, we report the properties of the heaviest neutron star,  $(M_{\max}^{\text{TOV}}, R_{\max}^{\text{TOV}})$ , its central density,  $n_{\max}^{\text{TOV}}$ , and the incompressibility at  $n_{\max}^{\text{TOV}}, K_{\max}$ .

EOS	$M_{\max}^{\text{TOV}}$ [ $M_{\odot}$ ]	$R_{\max}^{\text{TOV}}$ [km]	$n_{\max}^{\text{TOV}}$ [ $n_0$ ]	$K_{\max}$ [GeV]	Ref.	EOS	$M_{\max}^{\text{TOV}}$ [ $M_{\odot}$ ]	$R_{\max}^{\text{TOV}}$ [km]	$n_{\max}^{\text{TOV}}$ [ $n_0$ ]	$K_{\max}$ [GeV]	Ref.
ALF2	1.99	11.31	6.05	6.0	[21]	BA	2.60	12.39	4.72	12.4	[22]
BHB	2.10	11.59	5.94	8.2	[23]	BL	2.10	10.50	7.18	17.2	[24, 25]
BSK20	2.16	10.16	7.03	21.6	[26]	BSK21	2.27	10.99	6.09	16.3	[27]
CMF	2.10	11.58	5.94	8.3	[28]	CMFy	2.07	11.58	5.72	6.7	[29]
CMFy1	2.00	11.51	5.00	5.6	[29]	CMFy2	2.07	11.42	6.13	8.6	[29]
CMFy3	2.07	11.47	6.02	8.4	[29]	DD2	2.42	11.90	5.26	12.8	[30, 31]
DD2F-RDF (1.1)	2.14	10.21	7.17	16.5	[32]	DD2F-RDF (1.2)	2.16	10.95	6.42	7.09	[32]
DD2F-RDF (1.3)	2.04	10.37	7.28	10.74	[32]	DD2F-RDF (1.4)	2.03	10.21	7.27	10.86	[32]
DD2F-RDF (1.5)	2.04	10.34	7.27	10.63	[32]	DD2F-RDF (1.6)	2.02	10.09	7.64	13.81	[32]
DD2F-RDF (1.7)	2.13	10.81	6.67	8.37	[32]	DD2F-RDF (1.8)	2.07	10.22	7.30	10.38	[32]
DD2F-RDF (1.9)	2.17	10.78	6.44	6.69	[32]	DD2qG	2.15	12.53	5.11	2.6	[33]
DDH	2.16	11.19	6.09	8.4	[34]	DDHy	2.04	11.31	6.02	8.5	[35]
DD2hyp1	2.00	11.37	6.28	8.0	[36]	DD2hyp2	2.06	11.65	5.90	7.9	[36]
GM1	2.38	12.14	5.26	12.0	[37]	GM1y1	2.29	11.90	5.26	10.1	[35]
GM1y2	2.11	12.01	5.27	6.2	[35]	H3	1.70	11.17	6.84	4.7	[37–39]
H4	2.02	11.62	5.98	7.7	[37–39]	HB	2.45	11.59	4.21	14.8	[37–39]
HOLO	2.33	11.71	5.23	6.8	[40]	IUFSU	1.95	11.23	6.33	5.5	[41]
LS220	2.04	10.65	7.03	12.6	[42]	MPA1	2.47	11.28	5.49	23.6	[43]
MS1	2.76	13.26	4.21	7.5	[44]	NL3	2.79	13.38	4.11	13.9	[45]
OOS1	2.05	12.54	4.93	3.9	[46]	OOS2	2.12	12.72	4.74	4.0	[47]
OOS3	1.94	13.02	4.22	2.5	[47]	QHC18	2.04	10.36	7.07	10.5	[48]
QHC19A	1.92	10.21	7.48	9.5	[49]	QHC19B	2.06	10.51	6.85	10.2	[49]
QHC19C	2.18	10.73	6.43	11.0	[49]	QHC19D	2.27	10.83	6.21	11.9	[49]
SFHo	2.05	10.32	7.18	13.7	[50]	SFHx	2.13	10.74	6.59	10.3	[50]
SKa	2.20	10.90	6.39	17.0	[51]	SKb	2.18	10.62	6.62	17.1	[51]
Ski6	2.19	10.76	6.47	16.0	[51]	SLy4	2.05	10.01	6.47	13.6	[52]
SRO(0)	2.20	10.74	6.51	15.8	[33, 53]	SRO(2)	2.16	11.06	6.40	9.1	[33, 53]
SRO(3)	2.23	10.71	6.46	15.5	[33, 53]	SRO(4)	2.20	10.75	6.53	16.0	[33, 53]
SRO(5)	2.19	10.65	6.64	18.9	[33, 53]	SRO(6)	2.10	11.50	6.04	5.8	[33, 53]
SRO(7)	2.22	10.72	6.53	16.3	[33, 53]	SRO(8)	2.18	10.73	6.67	16.8	[33, 53]
TM1	2.21	12.56	5.15	6.4	[54, 55]	TM1-2	2.25	12.23	5.28	6.8	[56]
TM1-2q1	2.06	12.56	5.10	6.7	[56]	TM1-2q2	2.21	12.57	5.03	4.0	[56]
TM1-2y	1.98	12.27	5.42	4.7	[56]	TMA	2.02	12.27	5.60	5.3	[57]

Additionally, we repeat our  $q \neq 1$  analysis in terms of  $\mathcal{C}_{\max}^{\text{TOV}}$ . In the right panel of Figure 6, we present fits for the  $\alpha_{h,l}$  coefficients introduced in equation 2 of the main text in terms of  $\mathcal{C}_{\max}^{\text{TOV}}$ . The results are:

$$\begin{aligned}\alpha_l &= -(5.62 \pm 0.92)\mathcal{C}_{\max}^{\text{TOV}} + (1.94 \pm 0.26), \\ \alpha_h &= -(1.34 \pm 0.32)\mathcal{C}_{\max}^{\text{TOV}} + (0.390 \pm 0.091).\end{aligned}\quad (7)$$

The quality of the fits (estimated for example by the adjusted coefficient of determination,  $R_{\text{adj}}^2$ ) are comparable, but overall slightly worse than the ones obtained in the main text for  $K_{\max}$ :  $R_{\text{adj}}^2$  moves from 0.70 and 0.99 for the fits in  $K_{\max}$  to 0.76 and 0.88 for the fits in  $\mathcal{C}_{\max}^{\text{TOV}}$ , for

the high- and low- $q$  fits, respectively.

Finally, given the analogy between the definition of  $K$  (equation 1 of the main text) and the square of the speed of sound of NS matter,  $c_s^2 = \partial P / \partial \epsilon|_{T=0, \delta_{\text{eq}}}$ , where  $P$  and  $\epsilon$  are the pressure and the density of internal energy, and  $\delta_{\text{eq}}$  is the symmetry parameter for NS matter in neutrinoless weak equilibrium, we investigate also the relation between  $K_{\max}$  and  $c_{s,\max}^2$ , defined as the square of the speed of sound at  $n_{\max}^{\text{TOV}}$ . In the left panel of Figure 7 we present  $K_{\max}$  as a function of  $c_{s,\max}^2$  for all the EOSs in Table (II). With the exception of a few outliers, a linear relation between  $K_{\max}$  and  $c_{s,\max}^2$  holds. We perform

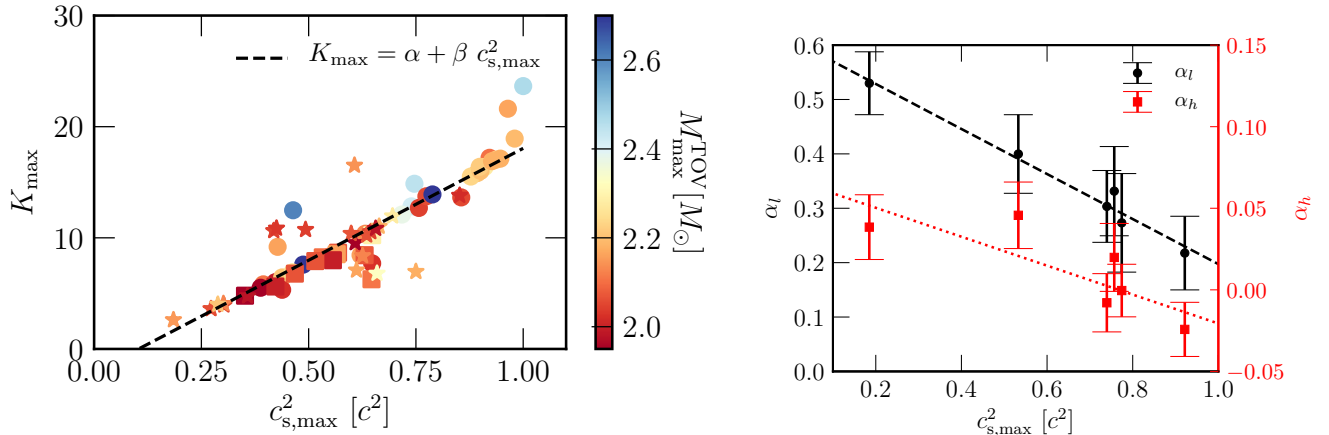


FIG. 7. Left:  $K_{\max}$  as a function of  $c_{s,\max}^2$  for the EOSs presented in Table (II). The dashed line correspond to a linear fit. Right: Slope parameters,  $\alpha_{h,l}$ , presented in the main text (see equations 2 and 3), as a function of the square of the speed of sound at  $n_{\max}^{\text{TOV}}$ ,  $c_{s,\max}^2$ . The dashed and dotted lines represent a linear fit with respect to  $c_{s,\max}^2$ .

a linear interpolation,  $K_{\max} = \alpha + \beta (c_{s,\max}/c)^2$ , finding  $\alpha = (-2.09 \pm 0.86)$  GeV and  $\beta = (20.1 \pm 1.3)$  GeV, with  $R_{\text{adj}}^2 = 0.78$ . For  $c_{s,\max}^2$  approaching unity, a possible divergence or an upper limit for  $K_{\max}$  are suggested. However, no firm conclusions can be drawn from the paucity of models and from the intrinsic limitation of non-relativistic nucleonic EOSs in modeling such a regime. Motivated by this result, we repeat our  $q \neq 1$  analysis also in terms of  $c_{s,\max}^2$ . In the right panel of Figure 7, we present fits for the  $\alpha_{h,l}$  coefficients introduced in equation 2 of the main text as a function of  $c_{s,\max}^2$ . The results are:

$$\begin{aligned}\alpha_l &= -(0.414 \pm 0.027)c_{s,\max}^2 + (0.611 \pm 0.018), \\ \alpha_h &= -(0.089 \pm 0.030)c_{s,\max}^2 + (0.068 \pm 0.022).\end{aligned}\quad (8)$$

Also in this case, the quality of the fits are comparable, but overall slightly worse, than the ones obtained in the main text for  $K_{\max}$ :  $R_{\text{adj}}^2$  is 0.60 and 0.95 for the high- and low- $q$  fits, respectively.

The study of the behavior of  $M_{\text{th}}(q)$  has been the subject of several recent works, that provided useful fits in different variables and according to different ansatz. Tootle *et al.* [60] and Kolsch *et al.* [61] used a definition of PC that is not equivalent to ours. Despite providing similar results, the average and the maximum variations between the two methods reported by Ref. [60] are larger than our numerical errors and comparable to the overall variation we are interested to model. Moreover, Ref. [60] studied the possible existence of a quasi-universal relation, while here we focus on a EOS dependent relation. Thus, we abstain from a detailed comparison with the results reported in these two works. On the other hand, our definition of PC is equivalent to the one used in [59] and thus we can compare our results with the polynomial fits discussed in [59] and presented

in their equation 10. In Figure 8, we compare our results with all the sets of fits ("b", "b+h", "b+e", "b+h+e") reported in their table VI for  $M_{\text{th}} = M_{\text{th}}(q, M_{\max}^{\text{TOV}}, R_{1.6})$  and  $M_{\text{th}} = M_{\text{th}}(q, M_{\max}^{\text{TOV}}, R_{\max}^{\text{TOV}})$ . We note that the fit in  $(q, M_{\max}^{\text{TOV}}, R_{1.6})$  predicts results that are, on average, closer to ours than the fit in  $M_{\text{th}}(q, M_{\max}^{\text{TOV}}, R_{\max}^{\text{TOV}})$ , despite the fact that the latter shares the same set of independent variables. However, for most of the EOSs, differences larger than our numerical uncertainties and than the fit residuals reported in [59] can be observed between the fits and our results in at least a portion of the relevant  $q$  interval. In particular, both the fits are not able to reproduce the slight increase in  $M_{\text{th}}(q)$  for  $q \lesssim 1$  for the BLh EOS, as also observed by Kolsch *et al.* for other EOSs [61].

- 
- [1] D. Radice and L. Rezzolla, *Astron. Astrophys.* **547**, A26 (2012), arXiv:1206.6502 [astro-ph.IM].
  - [2] D. Radice, L. Rezzolla, and F. Galeazzi, *Mon.Not.Roy.Astron.Soc.* **437**, L46 (2014), arXiv:1306.6052 [gr-qc].
  - [3] D. Radice, L. Rezzolla, and F. Galeazzi, *Class.Quant.Grav.* **31**, 075012 (2014), arXiv:1312.5004 [gr-qc].
  - [4] F. Löffler *et al.*, *Class. Quant. Grav.* **29**, 115001 (2012), arXiv:1111.3344 [gr-qc].
  - [5] S. Bernuzzi and D. Hilditch, *Phys. Rev.* **D81**, 084003 (2010), arXiv:0912.2920 [gr-qc].
  - [6] D. Hilditch, S. Bernuzzi, M. Thierfelder, Z. Cao, W. Tichy, and B. Bruegmann, *Phys. Rev.* **D88**, 084057 (2013), arXiv:1212.2901 [gr-qc].
  - [7] D. Pollney, C. Reisswig, E. Schnetter, N. Dorband, and P. Diener, *Phys. Rev.* **D83**, 044045 (2011), arXiv:0910.3803 [gr-qc].
  - [8] C. Reisswig, C. Ott, E. Abdikamalov, R. Haas,

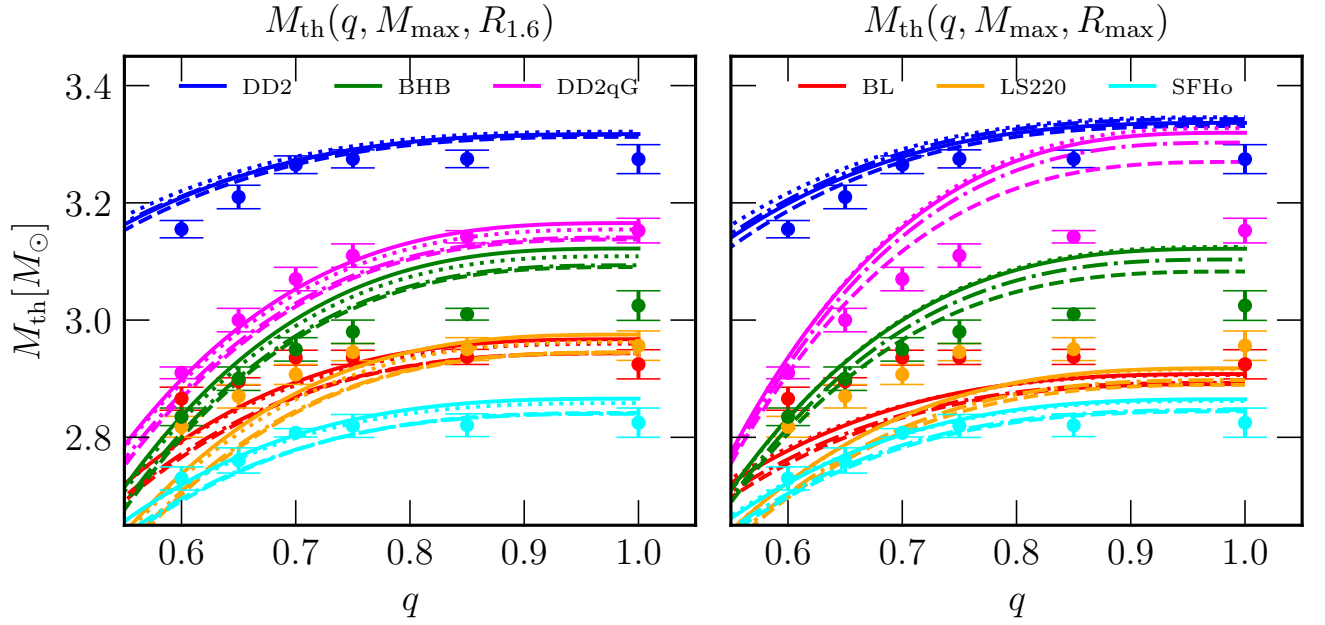


FIG. 8. Comparison between our results (dots) and the  $q$ -dependent fit results presented in [59], equation 10 and table VI. Different colors refer to the six EOS used in our work, while different lines correspond to different EOS samples employed in Table IV of [59]. In particular, we include the baseline "b" sample (solid), the "b+h" sample (dashed), the "b+e" sample (dotted) and the "b+h+e" sample (dash-dotted).

- P. Mösta, *et al.*, Phys.Rev.Lett. **111**, 151101 (2013), arXiv:1304.7787 [astro-ph.CO].
- [9] E. Schnetter, S. H. Hawley, and I. Hawke, Class.Quant.Grav. **21**, 1465 (2004), arXiv:gr-qc/0310042 [gr-qc].
- [10] M. J. Berger and J. Oliger, J.Comput.Phys. **53**, 484 (1984).
- [11] M. J. Berger and P. Colella, Journal of Computational Physics **82**, 64 (1989).
- [12] D. Radice, A. Perego, K. Hotokezaka, S. A. Fromm, S. Bernuzzi, and L. F. Roberts, Astrophys. J. **869**, 130 (2018), arXiv:1809.11161 [astro-ph.HE].
- [13] F. Galeazzi, W. Kastaun, L. Rezzolla, and J. A. Font, Phys.Rev. **D88**, 064009 (2013), arXiv:1306.4953 [gr-qc].
- [14] D. Radice, F. Galeazzi, J. Lippuner, L. F. Roberts, C. D. Ott, and L. Rezzolla, Mon. Not. Roy. Astron. Soc. **460**, 3255 (2016), arXiv:1601.02426 [astro-ph.HE].
- [15] E. Gourgoulhon, P. Grandclement, K. Taniguchi, J.-A. Marck, and S. Bonazzola, Phys.Rev. **D63**, 064029 (2001), arXiv:gr-qc/0007028 [gr-qc].
- [16] A. Bauswein, S. Goriely, and H.-T. Janka, Astrophys.J. **773**, 78 (2013), arXiv:1302.6530 [astro-ph.SR].
- [17] T. Dietrich, N. Moldenhauer, N. K. Johnson-McDaniel, S. Bernuzzi, C. M. Markakis, B. Brügmann, and W. Tichy, Phys. Rev. **D92**, 124007 (2015), arXiv:1507.07100 [gr-qc].
- [18] T. Dietrich, M. Ujevic, W. Tichy, S. Bernuzzi, and B. Brügmann, Phys. Rev. **D95**, 024029 (2017), arXiv:1607.06636 [gr-qc].
- [19] S. Bernuzzi *et al.*, Mon. Not. Roy. Astron. Soc. (2020), 10.1093/mnras/staa1860, arXiv:2003.06015 [astro-ph.HE].
- [20] A. Bauswein, S. Blacker, V. Vijayan, N. Stergioulas, K. Chatzioannou, J. A. Clark, N.-U. F. Bastian, D. B. Blaschke, M. Cierniak, and T. Fischer, Phys. Rev. Lett. **125**, 141103 (2020), arXiv:2004.00846 [astro-ph.HE].
- [21] M. Alford, M. Braby, M. W. Paris, and S. Reddy, Astrophys. J. **629**, 969 (2005), arXiv:nucl-th/0411016.
- [22] F. J. Fattoyev, J. Piekarewicz, and C. J. Horowitz, Phys. Rev. Lett. **120**, 172702 (2018), arXiv:1711.06615 [nucl-th].
- [23] S. Banik, M. Hempel, and D. Bandyopadhyay, Astrophys. J. Suppl. **214**, 22 (2014), arXiv:1404.6173 [astro-ph.HE].
- [24] I. Bombaci and D. Logoteta, Astron. Astrophys. **609**, A128 (2018), arXiv:1805.11846 [astro-ph.HE].
- [25] D. Logoteta, A. Perego, and I. Bombaci, (2020), 10.1051/0004-6361/202039457, arXiv:2012.03599 [nucl-th].
- [26] J. M. Pearson, S. Goriely, and N. Chamel, Phys. Rev. C **83**, 065810 (2011).
- [27] J. M. Pearson, N. Chamel, S. Goriely, and C. Ducoin, Phys. Rev. C **85**, 065803 (2012), arXiv:1206.0205 [nucl-th].
- [28] V. Dexheimer and S. Schramm, Astrophys. J. **683**, 943 (2008), arXiv:0802.1999 [astro-ph].
- [29] V. Dexheimer, R. Negreiros, and S. Schramm, Phys. Rev. C **92**, 012801 (2015), arXiv:1503.07785 [astro-ph.HE].
- [30] S. Typel, G. Ropke, T. Klahn, D. Blaschke, and H. H. Wolter, Phys. Rev. **C81**, 015803 (2010), arXiv:0908.2344 [nucl-th].
- [31] M. Hempel, T. Fischer, J. Schaffner-Bielich, and M. Liebendorfer, Astrophys. J. **748**, 70 (2012), arXiv:1108.0848 [astro-ph.HE].
- [32] N.-U. F. Bastian, Phys. Rev. D **103**, 023001 (2021), arXiv:2009.10846 [nucl-th].
- [33] R. Kashyap *et al.*, (2021), arXiv:2111.05183 [astro-ph.HE].
- [34] F. Douchin and P. Haensel, Astron. Astrophys. **380**, 151 (2001), astro-ph/0111092.
- [35] M. Oertel, C. Providência, F. Gulminelli, and A. R. Raduta, J. Phys. G **42**, 075202 (2015), arXiv:1412.4545 [nucl-th].
- [36] M. Fortin, S. S. Avancini, C. Providência, and I. Vidaña, Phys. Rev. C **95**, 065803 (2017), arXiv:1701.06373 [nucl-th].
- [37] N. K. Glendenning and S. A. Moszkowski, Phys. Rev. Lett. **67**, 2414 (1991).
- [38] B. D. Lackey, M. Nayyar, and B. J. Owen, Phys. Rev. D **73**, 024021 (2006), arXiv:astro-ph/0507312.
- [39] J. S. Read, C. Markakis, M. Shibata, K. Uryu, J. D. Creighton, *et al.*, Phys.Rev. **D79**, 124033 (2009), arXiv:0901.3258 [gr-qc].
- [40] N. Jokela, M. Järvinen, G. Nijs, and J. Remes, Phys. Rev. D **103**, 086004 (2021), arXiv:2006.01141 [hep-ph].
- [41] X. Roca-Maza, X. Vinas, M. Centelles, P. Ring, and P. Schuck, Phys. Rev. C **84**, 054309 (2011), [Erratum: Phys.Rev.C 93, 069905 (2016)], arXiv:1110.2311 [nucl-th].
- [42] J. M. Lattimer and F. D. Swesty, Nucl. Phys. **A535**, 331 (1991).
- [43] H. Müther, M. Prakash, and T. L. Ainsworth, Phys. Lett. B **199**, 469 (1987).
- [44] H. Müller and B. D. Serot, Nucl. Phys. **A606**, 508 (1996), arXiv:nucl-th/9603037 [nucl-th].
- [45] G. Shen, C. J. Horowitz, and S. Teige, (2011), arXiv:1101.3715 [astro-ph.SR].
- [46] K. Otto, M. Oertel, and B.-J. Schaefer, Phys. Rev. D **101**, 103021 (2020), arXiv:1910.11929 [hep-ph].
- [47] K. Otto, M. Oertel, and B.-J. Schaefer, Eur. Phys. J. ST **229**, 3629 (2020), arXiv:2007.07394 [hep-ph].
- [48] G. Baym, T. Hatsuda, T. Kojo, P. D. Powell, Y. Song, and T. Takatsuka, Rept. Prog. Phys. **81**, 056902 (2018), arXiv:1707.04966 [astro-ph.HE].
- [49] G. Baym, S. Furusawa, T. Hatsuda, T. Kojo, and H. Togashi, Astrophys. J. **885**, 42 (2019), arXiv:1903.08963 [astro-ph.HE].
- [50] A. W. Steiner, M. Hempel, and T. Fischer, Astrophys. J. **774**, 17 (2013), arXiv:1207.2184 [astro-ph.SR].
- [51] F. Gulminelli and A. R. Raduta, Phys. Rev. C **92**, 055803 (2015), arXiv:1504.04493 [nucl-th].
- [52] E. Chabanat, P. Bonche, P. Haensel, J. Meyer, and R. Schaeffer, Nucl. Phys. A **635**, 231 (1998), [Erratum: Nucl.Phys.A 643, 441–441 (1998)].
- [53] A. S. Schneider, L. F. Roberts, and C. D. Ott, Phys. Rev. **C96**, 065802 (2017), arXiv:1707.01527 [astro-ph.HE].
- [54] H. Shen, H. Toki, K. Oyamatsu, and K. Sumiyoshi, Nucl. Phys. **A637**, 435 (1998), arXiv:nucl-th/9805035.
- [55] M. Hempel and J. Schaffner-Bielich, Nucl. Phys. **A837**, 210 (2010), arXiv:0911.4073 [nucl-th].
- [56] D. Logoteta *et al.*, submitted to Eur. Phys. J. A (2022).
- [57] Y. Sugahara and H. Toki, Nucl. Phys. A **579**, 557 (1994).
- [58] A. Bauswein, T. Baumgarte, and H. T. Janka, Phys.Rev.Lett. **111**, 131101 (2013), arXiv:1307.5191 [astro-ph.SR].
- [59] A. Bauswein, S. Blacker, G. Lioutas, T. Soulannis, V. Vijayan, and N. Stergioulas, Phys. Rev. D **103**, 123004

- (2021), arXiv:2010.04461 [astro-ph.HE].
- [60] S. D. Tootle, L. J. Papenfort, E. R. Most, and L. Rezzolla, (2021), arXiv:2109.00940 [gr-qc].
- [61] M. Kölsch, T. Dietrich, M. Ujevic, and B. Bruegmann, (2021), arXiv:2112.11851 [gr-qc].